

## Line-Voltage-Regulators Optimization in Electric Power Quality

Ganesh Prasad Khuntia<sup>1</sup>, Rashmi Ranjan Panigrahi<sup>2</sup>, Sudhansu Bhusan Pati<sup>3</sup>, Debasis Nanda<sup>4</sup>

<sup>1,3,4</sup> Assistant Professor, Department of Electrical and Electronics Engineering, Gandhi Institute for Technology, Bhubaneswar, India

<sup>2</sup> Assistant Professor, Department of Electrical and Electronics Engineering, Gandhi Engineering College, Bhubaneswar, India

### ABSTRACT

The rapid expansion of distributed energy resources in the low voltage grid causes voltage limit violations, especially in rural areas with little electric load. To solve this issue without costly grid reinforcement, one approach is the use of smart devices such as line-voltage-regulators. However, the majority of these devices carry out stepped voltage adjustments, which cause a negative effect on the dynamic voltage characteristic. For this reason, this paper deals with a novel line-voltage-regulator and its power quality optimized control. The novel setup enables a continuous voltage regulation in a robust way by using variable inductors. The control design focuses on mitigating side-effects like harmonic distortion emission and increased grid impedance. Finally, a laboratory analysis evaluates the novel line-voltage regulator in comparison to a stepped one with regard to power quality.

**Keywords:** Line-voltage-regulation Low voltage grid Power quality Variable inductor Voltage control

### INTRODUCTION

The rapid expansion of distributed energy resources (DER) in the low voltage grid and the resulting reverse power flow cause voltage limit violations [8, 22], especially in rural grids with little electric load. To keep the voltage within the limits specified by EN50160 [1], but not to slow down this expansion, the low voltage grid needs to be improved. Grid reinforcements can be partly avoided using innovative devices, such as on-load tap changers and line-voltage-regulators (LVR) [18]. These devices control the line voltage directly without changing the reactive power flow. The majority of these devices carry out stepped voltage adjustments, such as those presented in [6] and [16]. However, this type of adjustments causes rapid voltage changes and thus lead to flicker effects [5]. Further negative effects due to rapid voltage changes are motor braking/acceleration, malfunction of control systems acting on the voltage angle and impairment of electronic equipment [19]. Alternatively, LVRs can be based on power electronics to enable a continuous voltage adjustment [3, 4, 7]. These devices can be quite powerful as they have a high control speed and can compensate various voltage issues. However, these devices usually emit high frequency harmonics [7]. Furthermore, power electronics have a relatively high failure rate [23]. Therefore, more maintenance and repairs have to be expected, which lead to high operating costs.

In this context, the InLiNe project analyzed the use of variable inductors (VI) as a novel technique for LVRs. The VI technique can merge a continuous voltage adjustment with a robust, cost effective design by avoiding power electronics. However, in a naive design the device

increases the grid impedance and emits harmonic distortions. To mitigate these effects an improved setup is constructed in laboratory [11]. Building on the constructed setup, this paper focuses on a control approach that provides a power quality (PQ) optimized operation. The control approach enables a continuous voltage regulation and mitigates the side effects of the novel LVR. To identify a suitable controller, a detailed model is constructed that considers the nonlinear behavior of the setup. A laboratory analysis validates the control system and evaluates remaining side effects with regard to PQ. Moreover, the results are compared to a measured, stepped voltage-regulation to illustrate the advantages of the continuous voltage-regulation.

All in all, this paper provides the setup and the controller development for a novel, PQ optimized LVR, which can be an effective application for the

distribution grid. The presented approaches for modelling and controlling can be adapted for other applications based on variable inductors as these applications are typically characterized by a nonlinear behavior due to the changing inductance. The laboratory analysis provides a detailed overview of the PQ effects on the grid and can be utilized to evaluate the use of an LVR for a specific grid section with voltage limit violations.

1. Setup and functionality

To understand the general concept of an LVR based on VIs, one needs to consider first its elementary structure. An LVR based on VIs is composed of a series transformer, whose primary winding is part of an inductive voltage divider, and a VI, which forms the second part of the

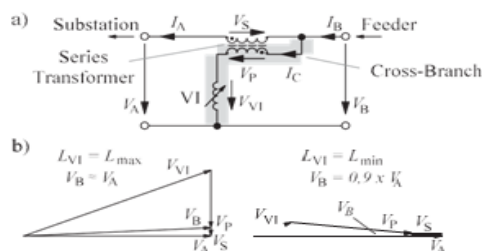


Fig. 1. Elementary design in voltage-reduction mode: a) Single-phase circuit b) Phasor diagrams for two VI control states.

voltage divider. The inductance of the VI can be reduced, which increases the voltage at the primary winding of the series transformer and its effect on the output line voltage. Depending on the transformer winding direction, voltage-boost mode or voltage reduction mode can be selected. Fig. 1a) shows a simplified single-phase circuit in voltage-reduction mode that can be used to compensate overvoltages caused by DER. Fig. 1b) shows the corresponding phasor diagrams for two VI control states. The voltages by different inductivities are depicted qualitatively. The presented elementary design is similar to the design patented in [21].

The elementary design has the main disadvantage of increasing the grid impedance in the initial state if the VI has a high inductance. This disadvantage results from dimensioning the cross-branch to prevent a power flow over the series transformer in this state. Because the initial inductance value of the VI must be chosen accordingly high, the series transformer is almost in no-load operation on the primary side. As a result, the magnetizing reactance of the series transformer has a high inductive impact on the grid impedance.

An increased grid impedance causes well-known effects such as a reduction of the short-circuit current and the interference immunity to PQ. Recent research also shows that frequency dependent grid impedance has a strong influence on harmonic stability of converters [10,24].

To avoid the grid impedance increase, a significant improvement is developed and published in [11]. According to this, Fig. 2 shows the improved LVR design. A second VI ( $VI_{Byp}$ ) is connected in parallel to the series transformer. By a maximal reduction of the  $VI_{Byp}$  inductance, the series transformer is nearly

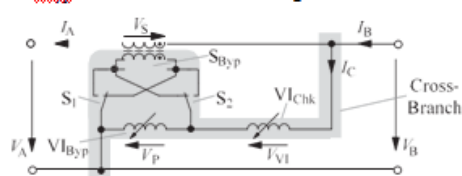


Fig. 2. Single-phase circuit of the improved LVR design [11].

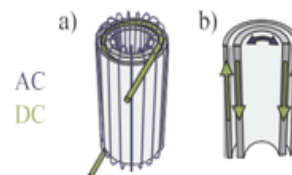


Fig. 3. VI design: a) Setup b) Magnetic flux in the core.

short-circuited. This reduction bypasses the influence of the transformer's magnetizing reactance. To enable a continuous LVR control, a combined control of  $VI_{chk}$  and  $VI_{Byp}$  is required. The control task is to ensure that the series transformer does not work in no-load operation. Yet, the impedance of the cross-branch should be still sufficient to limit the cross-current  $I_C$  to allow for compact components and less grid losses. Section 3 discusses this combined control approach in more detail. As a result,  $VI_{Byp}$  is an important tool to optimize the influence of the LVR on PQ.

In addition to the elements described before, Fig. 2 shows three switches. The switches  $S_1$  and  $S_2$  enable switching from voltage-reduction mode to voltage-boost mode by commutating the series transformer. The switch  $S_{Byp}$  enables short-circuiting the series transformer

to separate the influence of the LVR completely from the grid. By closing  $S_{BYD}$ , the LVR is turned to standby mode without any interruption in the distribution system. In this mode only the copper losses of the secondary winding occur.

Next, the setup and functionality of the used VI technique is considered. In principle, a VI can be built using a variety of techniques [12]. However, to enable a continuous and robust control, the best choice is a saturable reactor. In this technique, the core of an inductor is driven into saturation by an extra DC winding. The saturation reduces the permeability of the material. As a result, the inductance of the AC winding decreases proportionally. In a naive design, the DC flux only

generates a saturation effect in one of the two AC halfwaves. This leads to asymmetries in the AC signals. Furthermore, an unwanted voltage transfer from the AC to the DC winding occurs. To mitigate these effects, a variety of different designs exist [17].

The VI design utilized for the LVR presented here is patented in [9] and is illustrated in Fig. 3. This VI consists of an AC and a DC winding that are wound on two toroidal cores (Fig. 3a)). The two windings and the corresponding fluxes are orthogonal to each other (Fig. 3b)). Thus, the DC and AC windings are decoupled, and the saturation affects the AC signals symmetrically.

## 2. Combined control approach

In the following, a combined open-loop control of  $VI_{CHK}$  and  $VI_{BYD}$  is developed to enable a PQ optimized operation of the LVR. The combined control approach considers the minimization of the additional grid impedance while providing a continuous voltage regulation. In addition, the approach takes into account the reduction of power consumption by limiting the cross-current, and the mitigation of voltage disturbances generated by the saturation effects in the VIs. For this purpose, characteristic maps are determined with measurements. Each map takes into account one characteristic quantity depending on the control states of the VIs. Based on these maps, the best control path is selected.

The characteristic quantities as voltage variation  $\Delta V$ , cross-current  $I_C$  and output voltage distortions  $THD_V$  are measured during normal grid operation. Thereby, the voltage variation  $\Delta V$  corresponds to the difference between  $V_{B,RMS}$  and  $V_{A,RMS}$ . By short-circuiting the LVR output, the characteristic quantity of the additional grid impedance  $Z_{VR,grid}$  is determined.

Fig. 4 a) - d) shows the characteristic maps of the LVR in voltage-reduction mode by an inductive line-current. For voltage-boost mode, the maps are nearly

similar, only  $\Delta V$  changes polarity.

To understand the LVR behavior depicted in these maps, one needs

to remember that the voltage regulation of the LVR works by varying the voltage divider ratio between  $VI_{CHK}$  and the series transformer. A high DC control-current in  $VI_{CHK}$  reduces its inductance and leads to an increased voltage variation  $\Delta V$  at the LVR.  $VI_{BYD}$ , on the contrary, bypasses the impact of the series transformer. As a result, a high DC control-current in the  $VI_{BYD}$  reduces the LVR effects on the line.

Consequently, the initial operation point is achieved by a control state of  $VI_{CHK}$  at 0% (of  $I_{C,max}$ ) and  $VI_{BYD}$  at 100%. At this point, the LVR has nearly no effect on the line, and the variation of the output voltage is nearly zero. In contrast, the control state of  $VI_{CHK}$  at 100% and  $VI_{BYD}$  at 0% causes the maximal voltage variation by the LVR (see

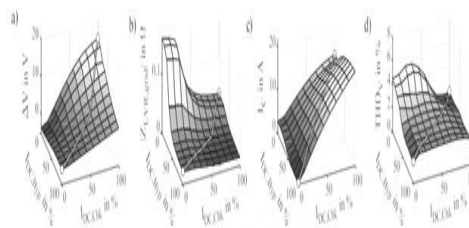


Fig. 4. Characteristic maps including the selected control path for the following characteristic quantities: a) Output voltage variation  $\Delta V = V_{B,RMS} - V_{A,RMS}$  b) Additional grid impedance  $Z_{VR,grid}$  c) Cross-current  $I_C$  d) Output voltage distortion  $THD_V$ .

Fig. 4a)).

For the control path, the control states of both VIs around 0% have to be avoided to minimize the impact of the magnetizing reactance of the series transformer on the grid (see Fig. 4b)). In addition, the control states of both VIs around 100% are prohibited to limit the cross-current  $I_C$  (see Fig. 4c)). For the combined control approach, the aim is to avoid the top 20% of  $I_C$ . Furthermore, the use of  $VI_{BYD}$  can reduce output voltage distortion  $THD_V$  caused by the saturation effects in the VI cores (see Fig. 4d)). Again, the top 20% of  $THD_V$  should be avoided.

Building on these constraints specified above, a control path is established and displayed in the characteristics maps. For the DC control current, the following functional relationship is obtained by a maximum control current of 1 A.

$$\begin{cases} -\leq I_{C,max} + 1 \text{ A} & \text{for } 0 \text{ A} < I_{C,max} < \leq \text{A} \\ I_C \leq \frac{3}{4} I_{C,max} + \frac{3}{4} \text{ A} & \text{for } I_{C,max} > \frac{3}{4} \text{ A} \end{cases} \quad (1)$$

Due to the selected control path, the additional grid impedance is lower than  $0.04 \Omega$  and the cross-current  $I_C$  is limited to 15 A. According to

similar control range (1% of the line voltage according to

### 3. Modelling

In addition to the control path developed in the previous section, a closed-loop control is required to regulate automatically the output voltage of the LVR. To identify a suitable controller, first a detailed model is constructed that considers the nonlinear behavior of the setup.

The modelling is divided into three parts. First, the LVR circuit and its mathematical relations are determined. The AC impedances of the two VIs are modeled in the first part.

The transfer behavior of the series transformer is modeled by using an ideal transformer. In addition, a parallel impedance  $Z_M$  represents the magnetizing reactance and the core losses of the series transformer. For simplicity, its winding joule losses and its leakage reactances are ignored since they have negligible influence on the LVR behavior. Each VI is represented by an impedance with a variable value. The impedance is varied by the core saturation caused by the DC flux. Since the DC currents generate this flux, the impedance

values can be expressed as a function of the DC currents  $Z_{Chk}(I_{DC})$  and  $Z_{Byp}(I_{DC})$ .

Based on this equivalent circuit, (2) is obtained for the input voltage

$V_A$  according to Kirchhoff's laws:

$$V = V_s + V_p + V_{VI} = a \cdot V_s + V_p + Z(I_{DC}) \cdot I$$

$$A \quad S \quad P \quad VI \quad P \quad Chk \quad DC \quad C \quad (2)$$

The voltage at the secondary side of the transformer is referred to the primary side.

The voltage at  $V_{Chk}$  and is also expressed by the cross-current  $I_C$  and the variable impedance  $Z_{Chk}(I_{DC})$ .

The voltage at the series transformer depends on the input current

$I$

As well as the cross-current  $I_C$  and can be calculated according to the superposition principle in (3):

$$V_p = -Z_p(I_{DC}) \cdot I_C - Z_p(I_{DC}) \cdot I_A$$

$$V_{p,VI} = a \cdot V_s \cdot I_A^2 \quad (3)$$

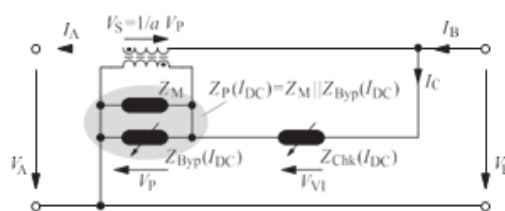
required as parameters in the LVR circuit and are modeled

in the second part by their dependency to the DC currents. The DC

The currents  $I_A$  and  $I_C$  generate two fluxes in opposite directions in the core. Each flux would inject a different voltage,  $V_{p,IC}$  and  $V_{s,IA}$ , at the transformer windings. The total voltage results from the superposition of these two voltages.  $Z_p(I_{DC})$  is the total impedance of  $Z_{Byp}(I_{DC})$  and  $Z_M$ . It is referred to the primary side. To calculate the voltage drop caused by  $I_A$ , the impedance

#### LVR Circuit

Fig. 5 shows the equivalent circuit of the LVR in voltage reduction mode. In this circuit, the series transformer and the VIs are modeled as



needs to be referred to the secondary side. However, the resulting voltage  $V_{s,IA}$  must be referred back to the primary side to get the total voltage for this side.

Inserting (3) in (2) and converting to  $I$  yields (4):

$$I_C = \frac{V_A + a \cdot V_s - Z_p(I_{DC}) \cdot I_A}{Z_p(I_{DC}) + Z_{Chk}(I_{DC})} \quad (4)$$

The output voltage  $V_B$  corresponds to (5):

$$V_B = V_s + V_{VI} = Z_p(I_{DC}) \cdot I_C - a \cdot Z_p(I_{DC}) \cdot I_A + Z_{Chk}(I_{DC}) \cdot I_C \quad (5)$$

Substituting  $I_C$  with (4) yields the required relation:

$$V_B = \dots$$

$V_B$

1

$$a \cdot Z_p(I_{DC}) + Z_{Chk}(I_{DC}) \quad (6)$$

It follows from (6) that  $V_B$  can be controlled by varying the VI impedances. However, there is a nonlinear relation. Additionally,  $V_B$  depends on input voltage  $V_A$  and on input current  $I_A$ .

The analogous procedure can be used to find the system equation for the voltage boost mode resulting in (7). The difference occurs because  $V_B$  has reversed polarity.

$$V_s = \frac{1}{s} Z_{VI}(s) I_{DC}$$

$$\frac{1}{s} \dots$$

$$\dots \frac{1}{s} Z_P \dots \}$$

VI Model: AC IMPEDANCE

For modelling the VI impedances, a black box model is derived by measurements. The purpose is to model the VI impedances as a linear component, which depends on the DC current.

It should be noted that modelling the VI impedances with a linear component is a simplification. Due to saturation effects in the VI core, the VI impedance doesn't behave linearly in every control state. Linearity exists only in an unsaturated core in the initial state and in a completely saturated core in the maximal reduction state. For the LVR, this means that voltages and currents in the cross-branch are distorted especially in the medium operating range. Here, the third, fifth and seventh harmonic occur in particular. However, the line voltage is hardly distorted since only a fraction of the distortions is added to the line voltage by the series transformer. Since only the relation between the output voltage  $V_B$  and the DC current is important for the control system design, it is acceptable to neglect the distortions in the cross-branch and to describe the VI impedances only with their total impedances. These total impedances can be calculated by the RMS quantities of measured voltages and currents.

For this purpose the LVR is driven into various control states on the combined control path from Section 3. Meanwhile, the cross-branch voltages and currents are measured. For the measurement the idling, there is no voltage at the series

(3). Based on these measurements, characteristic curves are determined

(b) the total impedance  $Z$  is considered ( $Z(I) =$  for the VI impedances, which are shown in Fig. 6a) and b). However, in

$$\frac{P}{Z_{ByD}(I_{DC})} \quad P \quad DC \quad Z_M$$

The depicted curves are obtained by averaging three different measurement series that are smoothed with spline interpolation.

According to the characteristic curves  $Z_{ca}$  shows a high

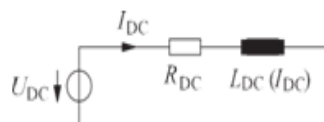


Fig. 7. Equivalent circuit of the DC winding of the VIs

To model the impedances, the characteristic curves are saved in look-up tables. By means of the measured copper losses  $R_{Chk} = 0.14 \Omega$ , the complex impedance can be provided for the model.

VI Model: DC circuit

Up to this point, the LVR model just represents the gain and phase shift behavior in steady state. In the following, the time behavior is added to the model. For that reason, the inductivity of the DC windings is considered. In the VI devices, the DC winding has a much higher inductivity than the AC winding due to a higher number of windings. Therefore, the charging and discharging time of the DC windings determine the time response of the LVR. However, the time response is not constant due to the variable permeability. Thus, the inductance of the DC winding also depends on the DC current itself. Because the DC circuits of the VIs are identical, the following model is used for both VIs. Fig. 7 demonstrates the equivalent circuit of the DC winding. In this circuit  $L_{DC}$  models the inductance and  $R_{DC}$  represents the joule losses, which are  $90 \Omega$  according to measurements. The circuit can be described with a differential equation and after Laplace Transform the following transfer function  $P_{DC}$  is obtained:

According to the characteristic curves  $Z_{CHK}$  shows a high impedance change at low DC currents. The reduction flattens even more with increasing DC current. The impedance range of  $Z_i$  is much smaller due to the influence of  $fZ_i$ . An open-circuit test with the series transformer [13] determines  $Z_i$  with approximately  $j16 \Omega$ . The common feature of both curves is that they achieve saturation with 1 A.

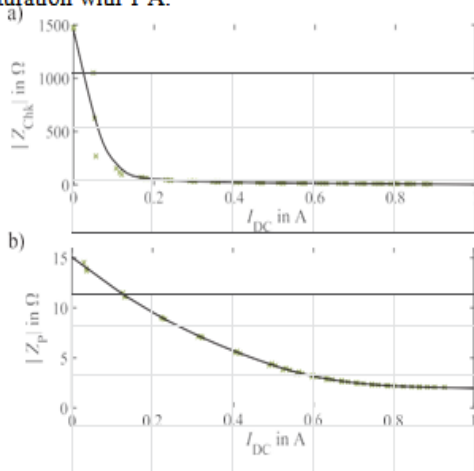


Fig. 8. Inductive behavior of the DC circuit:  
 a) Step responses of  $I_{DC}$   
 b) Characteristic curve of the DC inductivity  $L_{DC}$ .

Due to the dependency of  $L_{DC}$  to  $I_{DC}$ , the numerical solution of (8) is the most reasonable way for the model. Additionally, for  $L_{DC}$  ( $I_{DC}$ ), a look-up table is generated. For this purpose, step responses of  $I_{DC}$  are measured for different voltage intervals. Because a constant time response is assumed in each interval, time-constants  $\tau$  can be established according to a first-order differential equation. For this type of differential equation,  $\tau$  corresponds to the time until the step response reaches 63.2% of its final value [14].

Exemplary, Fig. 8a) shows the step response of  $I_{DC}$  for one measurement series. The point  $5 \cdot \tau$  is marked for each response (99.3% of the step response). Based on  $\tau$ , the inductance  $L_{DC}$  can be calculated for

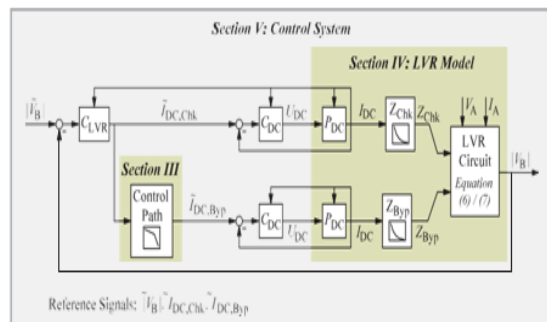
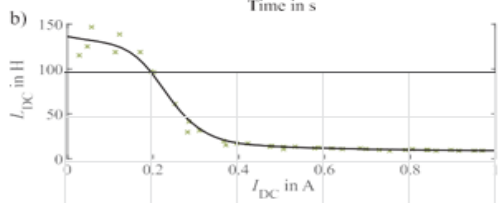
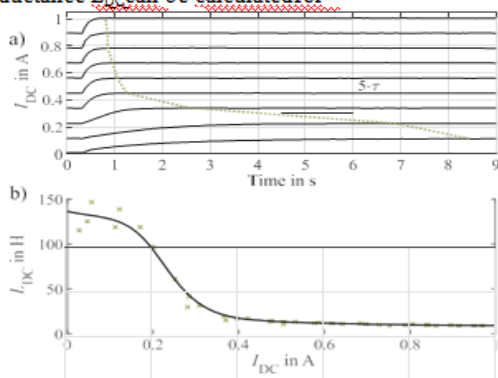


Fig. 9 Characteristic control system

each interval  $i$  according to (9).

$$LDC = \begin{matrix} i \in \{1, \\ RDC \cdot \tau_i \dots, n\} \end{matrix} \quad (9)$$

THESE INDUCTANCES ARE ASSIGNED TO THE AVERAGE VALUE OF THE CHOICE OF THE INTERVAL SIZE DETERMINES WHETHER THE LARGESIGNAL OR THE SMALLSIGNAL BEHAVIOR IS MODELLED MORE ACCURATELY. A COMPROMISE IS ATTEMPTED TO MODEL BOTH BEHAVIORS ADEQUATELY BY USING MEASUREMENT SERIES WITH 5V AND 10V INTERVALS. BASED ON THREE MEASUREMENT SERIES, A CHARACTERISTIC CURVE IS DETERMINED FOR THE LOOK-UP TABLE AND IS SHOWN IN FIG. 8b). AS ONE CAN SEE IN THIS FIGURE, THE DC INDUCTANCE ACTS SIMILAR TO THE AC IMPEDANCES AND DECREASES WITH HIGHER DC CURRENT AND REACHES SATURATION AT 1 A. WITH A DECREASING INDUCTANCE FROM 130 H TO 10 H THE CHARGING AND DISCHARGING TIME IS SHORTENED FROM AROUND 8 S TO 0.5 S.

#### 4. Control system design

behavior in time and gain response. The objective is to compensate these nonlinearities, resulting in a continuous and linear voltage regulation. For this purpose, a cascade-control system is developed (see Fig. 9). Two identical inner-loop controllers ( $C_{DC}$ ) control the DC currents of the VIs and also compensate the nonlinear time response. An outer-loop controller  $C_{LVR}$  tracks the set point, i.e. corrects disturbances, while compensating the nonlinear gain response. To design suitable controllers, desired closed-loop systems are defined for the inner-loops and the outer-loop. These desired systems are constrained by the feasible hardware range. Based on these desired systems and the LVR model, the controllers are computed.

For the two identical inner-loops, the desired time

the desired transfer function need to be lower than the inner-loop transfer function.

According to simulations, a time-constant of 5 s achieves good results and is used for  $H_{LVR}$ .

$$H_{LVR}(s) = \frac{1}{1.66s + 1} \quad (10)$$

$$LVR(s) = \frac{1}{5 \cdot s + 1} \cdot \frac{1}{1 + C_{LVR} P_{LVR}} \quad (12)$$

To obtain the outer-loop controller  $C_{LVR}$  from (12), first the new plant  $P_{LVR}$  needs to be derived.  $P_{LVR}$  combines the new time behavior, which is characterized by  $H_{DC}$  and the gain behavior  $K_{LVRSP}$  defined by the LVR circuit, which is depicted in Fig. 4a) as the control path

overlay. Because regarding on (1),  $I_{DC,SP}$  is fully dependent on  $I_{DC,CHK}$  and  $K_{LVR}$  depends only on  $I_{DC,CHK}$ . Thus, the new plant  $P_{LVR}$  is calculated as:

$$P_{LVR}(s) = \frac{K_{LVR}(I_{DC,CHK})}{DC(s)} \cdot H_{DC}(s) \quad (13)$$

Based on (12) and (13),  $C_{LVR}$  is obtained as follows:

$$C_{LVR}(s) = \frac{1.66 \cdot s + 1}{5 \cdot K_{LVR}(I_{DC,CHK})} \quad (14)$$

response is limited by the highest charging / discharging time of the DC circuits

DC 1.66

Overshooting the input signal  $U_{DC}$  would decrease this time, but this is not possible for discharging because the input signal  $U_{DC}$  is limited to 0V by the control hardware. For both inner-loops, a desired closed-loop system is defined as a first-order transfer function  $H_{DC}$  with the time constant  $T_{DC}$  of 1.66 s. This transfer function should be equal to the

$$H(s) = \frac{1}{1.66s + 1} \cdot C_{DC} \quad (10)$$

After inserting (8) in (10), the equation is

$$C(s) = \frac{L_{DC}(I_{DC}) \cdot s + 1}{I_{DC} \cdot R_{DC} \cdot (1.66s + 1)} \quad (11)$$

According to (11), a PI controller is obtained for  $C_{DC}$  that changes its parameter  $L_{DC}$  analog to the plant  $P_{DC}$ . Due to this variable parameter, the nonlinear time behavior can be compensated.

A desired closed-loop transfer function for the entire system  $H_{LVR}$  is defined for designing the outer-loop controller. To prevent instabilities,

Again a PI controller is obtained for  $C_{LVR}$  that changes its parameter  $K_{LVR}$  analog to the plant  $P_{LVR}$  and can therefore compensate the non-linear gain behavior.

Fig. 9 gives an overview of the control system representing the controllers and the model approach from the previous section.

The control system is validated in the simulation environment MATLAB / Simulink. In the control approach, the time response is chosen accordingly large that theoretically there is no overshooting of the control hardware limits. But, the simulation results show that the control signals get still constraints by the hardware limits if the error between the reference and the output signal is large. The hardware limits are set by the DC current source which supplies the DC circuit of the VIs. The DC current source has a range between 0-1 A at 0-90 V. Due to this limits and the time response, the controllers cannot compensate the nonlinear behavior of the LVR model completely. Furthermore, a non-linear behavior is visible, based on the simplifications in the VI models of the AC impedance and DC inductivity.

Nevertheless, the control system represents a good compromise between control speed and compensation of non-linearity

be sufficient for the control task.

However, windup effects on the PI controllers occur when the

system reaches its limits and can lead to unstable operation. To solve this issue, anti-windup systems are implemented for each PI controller. The used anti-windup system is based on backcalculation with gain  $M_{anti}$  [15] gives an overview of

such an anti-windup system and demonstrates its positive impact. The gain of the anti-windup system at  $C_{DC}$  is set to 0.1 and at  $C_{LVR}$  it is set to 100.

Next, the controller is validated in the laboratory with the LVR setup. For the validation, step responses of  $V_{A}$  are measured.

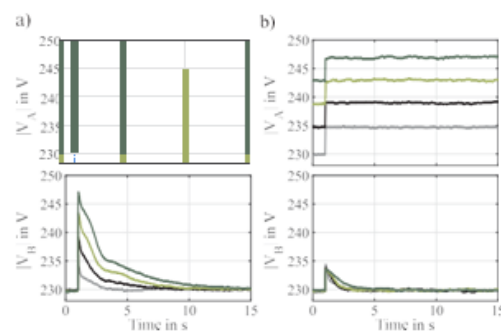


Fig. 10. Steps of  $V_A$  and responses of  $V_A$  a) Different step sizes b) Different starting voltages.

Theoretically, the step responses should be a decaying exponential function, but due to nonlinearities, the responses deviate as seen in Fig. 10a). This especially applies for steps larger than 10 V. For 4.5 V- steps, the control system acts nearly linear as seen in Fig. 10b). However, for these smaller steps the response is almost twice as fast as in the simulation. These deviations are caused by the simplifications during modelling. Evidently the DC inductance  $L_{DC}$  is modeled too large for small steps. In further approaches, parameter adjustment can be attempted to find a better compromise between the small- and large- signal behaviors.

All in all, the control behavior is satisfying, as the most non-

linearities are compensated. Moreover, the control system is at least as robust with a control time less than 10s, and as the control accuracy is lower than 1 V without overshooting. Due to the anti-windup system, good stability is achieved even when the control range is exceeded.

### 5. Power quality analysis

The novel LVR with the developed control system is evaluated regarding to its influence on PQ. For this purpose, the usage of the novel LVR is compared to the usage of a stepped LVR. For reference, a setup without any LVR is also measured.

For the PQ analysis, a test-grid is configured in the laboratory infrastructure of the smart-grid-ec-lab at the ipz[20], which is depicted in Fig. 11. A power amplifier is connected via a 300 m cable and a transformer to the external grid. Depending on the setup, an LVR technique can be linked in series between the line and the power amplifier.

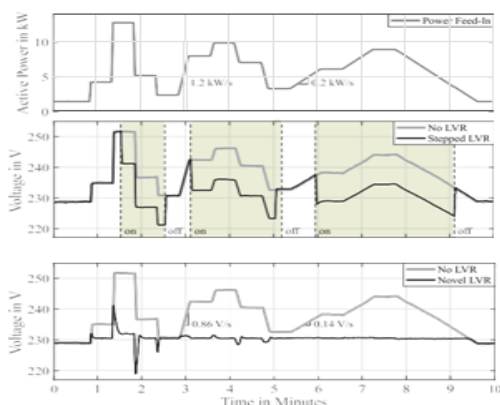


Fig. 12. Single-phase power feed-in and the resulting voltages of busbar (B) for the different setups.

Table 1

PQ Parameters for the analysed Voltage Sequences (mean  $\pm$  standard deviation) and requirements of standard \*EN50160[1], \*\*EN 61000-2-2[2].

Case	Voltage in V	THD <sub>v</sub> in %	Flicker P <sub>st</sub>
All Cases at (A)	250 $\pm$ 0.3	1.9 $\pm$ 0.03	0.1
Without LVR at (B)	239 $\pm$ 5.3	2.0 $\pm$ 0.06	0.9
Stepped LVR at (B)	233 $\pm$ 3.8	2.0 $\pm$ 0.05	1.6
Novel LVR at (B)	251 $\pm$ 0.6	2.4 $\pm$ 0.13	0.9
Standard	230 $\pm$ 10%*	$\leq 5$ %	$\leq 1$ **

This paper focuses on the issue of voltage rise due to the feed-in of DER, i.e. the analysis considers the LVR operation in voltage reduction mode. For the feed-in, the power amplifier generates an active power signal with different gradients of power change. The resulting line current causes a voltage drop at the cable. As the voltage at bus bar (A) is kept constant by the external grid, the voltage at bus bar (B) increases.

Fig. 12 illustrates the single-phase power feed-in and the resulting voltages at busbar (B) for the different setups. For the measured voltage sequences, the mean voltages with standard deviations are given in Table 1. Additionally, the voltage distortion THD<sub>v</sub> and the shor-

term

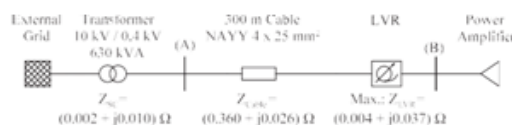


Fig. 11. Configuration of the test grid.

flicker P<sub>st</sub> (weighted 10 min mean) are listed. For comparison, the respective requirements of the standard are given last.

In the reference setup, the voltage signal at bus bar (B) tracks the power signal. With the usage of an LVR, the voltage rise at bus bar (B) should be compensated. The stepped LVR can reduce the line voltage by 10 V. It switches on at 236 V and switches off at 225 V with a delay of 10 s. With this mechanism, the mean voltage decreases by 6 V for the chosen feed-in scenario. Nevertheless, the on-off control of this LVR amplifies the voltage fluctuations and emits additional flicker. For this scenario, the flicker even exceeded the required value of 1%.



The novel LVR adjusts the voltage at busbar (B) in a continuous way by tracking a set-point of 230 V. Due to the slow control, rapid voltage variations initially result in control deviations, which are gradually compensated. However, gradients of 0.14 V/s can be completely compensated. With a voltage rise above 250 V the control range of the new LVR is exceeded, but still the voltage is reduced with the maximum range of 20 V. As the voltage follows a set-point, there are less voltage fluctuations and the dynamic voltage characteristic is improved. As a result, the mean voltage decreases about 8 V without amplifying the flicker value. The setup has the highest THD<sub>v</sub> caused by the saturation effects in the VIs. However, due to the optimized combined control presented in Section 3 the THD<sub>v</sub> is lower than in comparable LVR devices based on VIs [11] and clearly complies with the requirement.

Via the grid impedance, the voltage interferences expand primarily to the subordinate feeder section and thus the PQ at busbar (A) is not influenced by the LVRs.

### CONCLUSION

This paper dealt with a novel LVR and its PQ optimized regulation. The novel LVR is distinguished by the use of the VI technique, which enables a robust and continuous control. Three results have been provided in the course of this paper.

First, a detailed model is presented, which considers the nonlinear behavior of the novel LVR. In this paper, the model is necessary for the control design. Besides that, the model can be used later for dynamic RMS simulations. However, it got evident that the signal behavior of the model does not completely match the LVR in laboratory. In further approaches, parameter adjustment can be attempted to find a better compromise between the small- and large-signal behaviors.

Second, the control approach for a PQ optimized regulation has been given. Based on the open-loop control, side effects are mitigated to an acceptable level. This is achieved by specifying a combined control for both VIs which avoids undesirable control states. The additional closed-loop control proves to be robust and suitable for the desired control task and compensates most of the nonlinearities.

Third, the laboratory analysis evaluated remaining side effects of the novel LVR with regard to PQ and the results were compared to the usage of a stepped LVR. According to the analysis, both LVRs improve the static voltage characteristic. While the stepped LVR amplifies the voltage fluctuations and emits additional flicker, the novel LVR does not generate such kind of interferences, although there is still some harmonic distortion emission. Thus, the deployment of a simpler stepped LVR can be feasible in some situations, but it is advisable to choose an LVR with less side effects like the novel LVR presented in this paper if the corresponding PQ parameters require it.

Conclusively, this paper provided the conditions for the upcoming field test in a distribution system which is the final part of the InLiNe project. Additionally, the model provided in this work can be used to carry on the analysis of the novel LVR in different directions. For example, it would be possible to examine the control of voltage unbalances or the interoperability with other voltage regulation equipment.

### Declaration of Competing Interest

The authors declare that they have no known competing financial interests or personal relationships that could have appeared to influence the work reported in this paper.

### Acknowledgements

The InLiNe Project is funded by the German Federal Ministry for Economic Affairs and Energy.

## REFERENCES

- [1] EN50160:2010 Voltage characteristics of electricity supplied by public distribution system.
- [2] EN 61000-2-2:2002 + A1:2017, Electromagnetic compatibility (EMC) – Part 2-2: Environment– Compatibility levels for low frequency conducted disturbances and signalling in public low-voltage power supply systems.
- [3] G. Alain, R. Dominique, H.P. Biner, AC line voltage controller for grid integration of renewable energy sources, European Conference on Power Electronics and Applications, (2015). Geneva, France
- [4] P. Alcarria, S.F. Pinto, J.F. Silva, Active voltage regulators for low voltage distribution grids: The matrix converter solution, International Conference on Power Engineering, Energy and Electrical Drives (POWER ENG), (2013). Istanbul, Turkey
- [5] J. Barros, et al., Rapid voltage change in power system networks and their effect on flicker, IEEE Trans. Power Deliv. 31 (1) (2016) 262–270.
- [6] M. Carlen, et al., Line voltage regulator for voltage adjustment in MV-grids, CIRED Conference, (2015). Lyon, France
- [7] A. Garces, A. Trejos, A voltage regulator based on matrix converter for smart grid applications, IEEE PES Conference on Innovative Smart Grid Technologies (ISGT Latin America), (2011). Medellin, Colombia
- [8] M.M. Haque, P. Wolfs, Review of high PV penetrations in LV distribution networks: present status, impacts and mitigation measures, Renew. Sustain. Energy Rev. 62 (2016) 1195–1208.
- [9] E. Haugs, F. Strand, Magnetic controlled current or voltage regulator and transformer, (2001). WO2001090835A1 PCT/NO01/00217, Nov 29
- [10] M. Höckel, et al., Measurement of voltage instabilities caused by inverters in weak grids, CIRED Conference, (2017). Glasgow, UK
- [11] M. Holt, G. Grosse-Holz, C. Rehtanz, Line voltage regulation in low voltage grids, CIRED Workshop, (2018). Ljubljana, Slovenia
- [12] R. Hooper, B. Guy, R. Perrault, A current-controlled variable inductor, IEEE Instrum. Meas. Mag. 14 (4) (2011) 39–44.
- [13] W.G. Hurley, W.H. Wolfe, Transformers and Inductors for Power Electronics - Theory, Design and Applications, John Wiley & Sons Ltd, Chichester, UK, 2013, pp.228–230.
- [14] B.G. Lipták, Process Control and Optimization, 4th, Taylor & Francis, Boca Raton, Fla.: USA, 2005, p.100.
- [15] M.A.A. Murad, A. Ortega, F. Milano, Impact on power system dynamics of PI control limiters of VSC-based devices, 20th Power Systems Computation Conference, (2018). Dublin, Ireland
- [16] M.A. Pelegrini, et al., A portable voltage regulator as an innovative smart grid solution, IEEE PEST&D Conference and Exposition, (2014). Chicago, IL, USA
- [17] M.S. Perdigão, M.F. Menke, A.R. Seidel, R.A. Pinto, J.M. Alonso, A review on variable inductors and variable transformers: applications to lighting drivers, IEEE Trans. Ind. Appl. 52(1) (2016) 531–547.
- [18] H. Rui, et al., Guidelines for the integration of voltage control applications, International ETG Congress 2015: Die Energiewende – Blueprints for the New Energy Age, IEEE, Piscataway, NJ, 2015.
- [19] J. Schlabbach, E. Blum, T. Stephan, Voltage Quality in Electrical Power Systems, Institution of Electrical Engineers, London, 2001, pp.115–116.
- [20] A. Spina, et al., Smart grid technology lab – a full-scale low voltage research facility at TU Dortmund university, AEIT International Annual Conference, (2018). Bari, Italy
- [21] R. Tjeldhom, E. Haugs, F. Strand, System for Voltage Stabilization of Power Supply Lines, (2004). WO2004053615A1 PCT/NO2003/000417, Jun 24
- [22] R.A. Walling, R. Saint, R.C. Dugan, J. Burke, L.A. Kojovic, Summary of distributed resources impact on power delivery systems, IEEE Trans. Power Deliv. 23(3) (2008) 1636–1644.
- [23] H. Wang, M. Liserre, F. Blaabjerg, Toward reliable power electronics: challenges, design tools, and opportunities, IEEE Industrial Electronics Magazine, vol. 7, (2013), pp.17–26.
- [24] X. Wang, F. Blaabjerg, Harmonic stability in power electronic-based power systems: concept modeling and analysis, IEEE Trans. Smart Grid 10(3) (2019) 2858–2870.